CEAI, Vol.24, No.2, pp. 13-23, 2022 Printed in Romania

Flexible Joint Robot Manipulators Control using Fish Swarm Algorithm and Adaptive Inverse Control

Y. Xu, M. Yu, Y. Li

Department of vehicle and mechanical engineering, Changchun University, Jilin,China
(Corresponding author e-mail: 962182670@qq.com).

Abstract: Parameters uncertainties and disturbances broadly exist in robotic arms,especially for the flexible joint system in the process of manipulator movement,which terribly deteriorate system control performance.Thus a controller with parameter adaption is proposed for flexible joint system in this paper. First, the collision model and friction model of flexible rotary joint with clearance were established, and the global dynamics equation of manipulator was derived by generalized α method Secondly, the pre-applied joint torque is taken as the research object, and the fish swarm algorithm is used in MATLAB/SIMULINK module to optimize the PID (proportional-integral-differential)parameters and combined inverse control to reduce the impact vibration.Under real experimental conditions, the results show that the control torque curve is close to the pre-set curve, the amplitude is reduced, the vibration time is shortened within 1 second, and the influence of the joint clearance on the finished surface is reduced, which proves that the proposed method is feasible and the response speed is fast and can meet the requirements.

Keywords: robotics; adaptive control; inverse control; torque control; PID; fish swarm algorithm

1. INTRODUCTION

During the movement of the mechanical arm, the inevitable collision with the surrounding environment or within the interior of the mechanism can cause the speed to change suddenly and it affects the dynamic characteristics of the entire system. Therefore, it is necessary to control the entire system, especially rotating manipulator joints to reduce the impact (Adelhedi et al., 2015; Zhou et al., 2019; Ahmed et al., 2020).

The adaptive control (Song et al., 2018; Chien et al., 2007), the inverse control (Niţulescu, 2007), the PID control (Kalaivani et al., 2014) are used as the basic control method. Many new control algorithms are developed by experts by combining different control method, such as adaptive sliding control (Huang et al.,2004), Fuzzy logic control (Zirkohi et al., 2013), neural network (Talebi et al., 2002), adaptive neural network sliding mode controller (Sefriti et al., 2012) and decentralized direct adaptive fuzzy control (Fateh et al., 2013).

The integration of multiple control method effectively offset the disadvantages of single control method. The developed control system can propose two methods for reducing the numbers of rules and number of fuzzy inputs, which significantly reduce the computational complexity (Ahmed et al., 2020; Guo and Woo, 2003) and can perform well when the parameters are known (Vermeiren et al., 2012; Mustapha et al., 2014 and Yang et al., 2007), but when the parameters are changed or they cannot determined, these controller cannot adjust its parameters and get acceptable performance. Thus, the adaptive control can be the solution. The control method could change its character to respond the changeable environments (Omer et al., 2018).

PID as one of the most classic methods are employed in industry because of its capability to perform well. However, more and more complex system demands the redesign of PID control scheme (Sylvainet al., 2018). Thus, the combination of parameter optimization algorithm and PID were addressed by researchers in recent years. The original and simple event based PID control method was proposed by (Arzen, 1999). When the system is highly nonlinear and complex, the PID controller isn't effective because the varying conditions, while the Nonlinear PID could erase the drawback by adjust the nonlinear input and output. (Prakash and Srinivasan, 2009) have also discussed about that the N-PID controller design for the nonlinear model improves the closed loop performance. Due to the change of process parameters, the traditional N-PID system is improperly set, resulting in oscillation response and poor robust behavior. To achieve the satisfactory performance, it is necessary to optimize the parameter of PID. (Rajinikanth and Latha, 2012) have presented a controller parameter optimization for nonlinear systems using Enhanced Bacterial Foraging Algorithm (E-BFA).

Motivated by above papers, the following problems are expected to be resolved in this paper: (1) avoid the influence of joint space on the manipulator; (2) achieve excellent positioning performance within tiny error. Therefore, a inverse controller with parameter adaption is proposed for flexible joint system in this paper. Compared with the previous method to control the vibration of the trajectory through different composite control methods, the vibration by directly controlling torque to restrain during machining is considered. Firstly, the collision model and friction model of flexible joint are established, and the whole mechanical arm equation is derived and solved by generalized α method. To reduce the impact, in addition to set up the elastic compensation device in joints, the fish algorithm was used for PID optimization parameters, combining with the adaptive inverse control method. Simulation control was carried out for the manipulator with pre-added torque to make the control torque curve approach the pre-added torque curve continuously, so as to achieve rapid suppression of vibration. Meanwhile, to further verify the reliability of the control method, different gaps were set for the manipulator joints. The results show that the displacement curve after control is close to the ideal trajectory.

The organization structure is as follows: Section 2 presents the problem formation and sets dynamic model. Section 3 presents the design process and theoretical results of adaptive inversion law of controller proposed in this paper. Section 4 provides the simulation settings and comparison of results. Section 5 discusses the conclusion.

2. DYNAMIC MODEL AND PROBLEM FORMULATION

In the process of design, installation and processing, the joints will inevitably produce clearance. The clearance of the rotating pair is shown in Figure 1,where the shaft of the rotating pair is offset due to the existence of the clearance during the movement.

$$c = R_j - R_i \tag{1}$$

where c is the clearance size, R_i is the radius of axis, and R_j is the radius of bearings. O_{11}, O_{21} are the section centers of the rotating shaft and bearing respectively. P is the contact point, F_{rn}, F_{ri} are the normal force and tangential force in contact collision respectively.

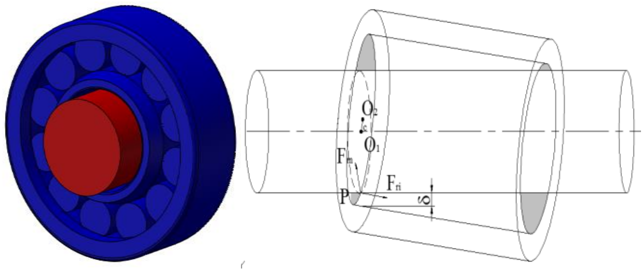

Fig. 1. Extrusion deformation diagram of clearance pair.

2.1 Rotary Pair Clearance Collision Model

Since there is a gap in the rotating pair during the movement, the center points of the shaft and the bearing do not coincide, so there will be three phases: free movement, contact and collision. The contact collision force is mainly divided into tangential friction force and normal collision force.

2.1.1 Normal impact force model

At present, the basic model of collision force is mainly the Hertz model, but it ignores the energy loss in the collision process. Therefore, researchers have further studied and proposed the Kelvin-Voigt model, the Hunt-Crossley model and the Lankarani-Nikravesh model.

Compared with the other two models, the Lankarani-Nikravesh collision force model considers the energy loss caused by elastic deformation and believes that the energy loss in the collision process is mainly caused by damping.

$$F_N = K\delta^n + D\dot{\delta} \tag{2}$$

where K is the stiffness coefficient, δ stands for the depth of impact puncture, n represents the nonlinear exponent. For the parabolic distribution of contact stress, like metal materials, n usually takes 1.5. D represents the damping coefficient, and $\dot{\delta}$ is the relative deformation velocity. The first term of (2)is the elastic deformation force based on the Hertz theory, and the second term is the energy loss caused by contact and collision, which is called damping force.

The damping coefficient D is expressed as follows:

$$D = \eta\delta^n \tag{3}$$

where η is the viscous damping factor that can be obtained according to the energy loss formula:

$$\eta = \frac{3K(1-c_e^2)}{4\delta^{(-)}} \tag{4}$$

where c_e is the recovery coefficient,and $\delta^{(-)}$ is the relative initial velocity at the point of impact.

$$F_N = K\delta^n\left[1 + \frac{3(1-c_e^2)}{4\delta^{(-)}}\right] \tag{5}$$

2.1.2 Tangential friction model

When the moving pair objects collide non-vertically, the shaft and the bearing will produce normal and tangential velocities at the collision point. The tangential velocity is caused by friction.

According to the Coulomb friction model, we can get

$$F_T = -\mu_d F_N \tag{6}$$

where μ_d is the friction coefficient.

Since the velocity of the Coulomb model changes from static friction to dynamic friction, (6)does not match the actual situation. Therefore, an improved Coulomb model is proposed.

$$\mu(v_t) = \begin{cases} -\mu_d\, sign(v_t) & |v_t| > v_d \\ -step(|v_t|, v_d, \mu_d, \mu_s) sign(v_t) & v_s \le |v_t| \le v_d \\ step(v_t, -v_s, \mu_s, v_s, -\mu_s) & |v_t| < v_s \end{cases} \tag{7}$$

where μ_s is static friction coefficient, μ_d is the kinetic friction coefficient, v_s is the static translation velocity, and v_d is the friction translation velocity.

Then, the modified Coulomb friction model is expressed as

$$F_T = -\mu_d F_N \, sign(v) \tag{8}$$

2.2 Dynamics of manipulator with joint clearance

When the joint space is not taken into consideration, the dynamics are as follows,

$$\begin{cases} M\ddot{x} + Kx + \varphi_q^{\ T} \lambda = F \\ \varphi(x,t) = 0 \end{cases} \tag{9}$$

where M is the mass matrix, x is the coordinate matrix, K is the stiffness matrix, φ_q is the Jacobian matrix of the constraint equation, λ is the Lagrange multiplier sub-matrix, F is the generalized force matrix and φ is constraint equations.

When the mechanism with clearance hinge rotates, the constraint equation is no longer applicable, and additional equations need to be introduced to restrict it.

$$\phi(e,t) = 0 \tag{10}$$

where e is the eccentric distance between the shaft and the bearing.

2.3 Solution of dynamic equation

The generalized α solution, which was built on Newmark, can not only maintain the response on the low frequency band, but also control the high frequency band(Chung J, Hulbert G M.,1993).The details are as follows:

$$\begin{cases} \alpha_0 = q_0^{''} = \ddot{x}_0 \\ (1-\alpha_i)\cdot\alpha_{n+1} + \alpha_i \cdot \alpha_n = (1-\alpha_f)\cdot q_{n+1}^{''} + \alpha_f \cdot q_n^{''} \end{cases} \tag{11}$$

where α is quasi-acceleration vector parameters.

The equation is solved and obtained,

$$\begin{aligned} q_{n+1} &= q_n + \Delta t \cdot q_n^{'} + \Delta t^2 \cdot ((\frac{1}{2} - \beta)\cdot \alpha_n + \beta \cdot \alpha_{n+1}) \\ q_{n+1}^{'} &= q_n^{'} - \Delta t \cdot (1-\gamma)\cdot \alpha_n + \gamma \cdot \Delta t \cdot \alpha_{n+1} \end{aligned} \tag{12}$$

Δt is integral step, γ, β are algorithm parameters and they could affect the calculation efficiency and accuracy. In additional,

$$\alpha_i = \frac{2\rho - 1}{\rho + 1}, \alpha_f = \frac{1}{\rho + 1}, \beta = \frac{1}{4}(1+\alpha_f - \alpha_i)^2, \gamma = \frac{1}{2} + \alpha_f - \alpha_i \tag{13}$$

$\rho \in [0,1]$,which is the spectral radius of the algorithm and it determines the distribution range of dissipated energy of the algorithm. When ρ =1,the generalized α method degenerates into gradient algorithm; When $\alpha_i = \alpha_f$ =0,the generalized α method degenerates into Newmark method; When α_i =0,the generalized α method degenerates into HHT method (Ortega et al., 2017).

The detailed flow chart is shown in Figure 2.

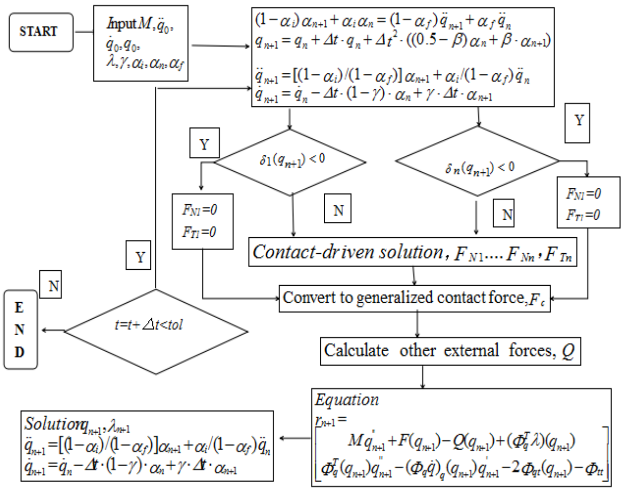

Fig. 2. Flowchart of generalized α solution.

(1) Establish system code. MATLAB is used to compile the mass matrix and displacement vector matrix of each unit, which is assembled into the generalized matrix of the system, and the initial value of simulation calculation is given.

(2) Predict generalized coordinates of nodes. Based on the relevant calculation criteria of generalized α method, predict the generalized coordinate matrix q_{n+1}, generalized velocity matrix $\dot{q}_{n+1}$ and acceleration matrix $\ddot{q}_{n+1}$ at the next moment t_{n+1}.

(3) Calculate contact deformation δ. According to the generalized coordinate matrix of the system and the distance of contact points between axis and bearings *d*, it can be calculated.

(4) Determine whether a contact collision has occurred. If $\delta(q_{n+1}) < 0$, the collision didn't occur; otherwise, it occurred, then using (5), (8), we calculated F_N, F_T.

(5) Calculate the generalized contact force matrix F_c.The force at each hinge contact point is converted to the force at element node, and the element force array is further assembled into the generalized contact force array of the system.

(6) Calculate the external force, Q.

(7) Solve the nonlinear equations with q_{n+1} as unknown variable. The generalized coordinate matrix q_{n+1} and Lagrangian matrix λ_{n+1} at t_{n+1} are obtained. According to (12), generalized velocity matrix $\dot{q}_{n+1}$ and acceleration matrix $\ddot{q}_{n+1}$ are solved.

(8) Repeat (2)-(7) until the running time reaches the simulation termination time.

2.4 Dynamic analysis

According to the collision model and hinge gap model established above, the impact of the clearance on the robotic arm is very severe, and the nonlinear effect at the joint is strong. Therefore, using the data of Table 1 could set the joints equation and the displacement curves of different clearances were thus painted.

Table 1. Structural parameters of manipulator dynamic analysis.

	mass/ kg	the position of the center of mass relative to the link coordinate system/m	inertia tensor /kg· m^2
Link 1	8.69	[0.0018,0.037,0.012]	$\begin{bmatrix} 0.086 & 0 & 0 \\ 0 & 0.086 & 0 \\ 0 & 0 & 0.019 \end{bmatrix}$
Link 2	8.65	[0.0018,0.037,-0.012]	$\begin{bmatrix} 0.261 & 0 & 0 \\ 0 & 0.296 & 0.388 \\ 0 & -0.388 & 0.236 \end{bmatrix}$
Link 3	6.43	[0.0028,0.0028,0.00003]	$\begin{bmatrix} 0.67 & 0 & -0.22 \\ 0 & 0.587 & 0 \\ 0.22 & 0 & 0.666 \end{bmatrix}$
Link 4	6.43	[0.0027,0.0027,0.0003]	$\begin{bmatrix} 0.58 & 0 & 0 \\ 0 & 0.576 & 0 \\ 0 & 0 & 0.578 \end{bmatrix}$
Link 5	5.96	[0.0018,0.0018,0.0030]	$\begin{bmatrix} 0.132 & 0 & 0 \\ 0 & 0.512 & 0 \\ 0 & 0 & 0.132 \end{bmatrix}$
Link 6	5.96	[0.0018,0.0018,0.0030]	$\begin{bmatrix} 0.132 & 0 & 0 \\ 0 & 0.512 & 0 \\ 0 & 0 & 0.132 \end{bmatrix}$

As a nonlinear system, the dynamic response of the joint with hinge clearance is very sensitive to joint clearance. The angular acceleration of the manipulator will suddenly change due to the existence of joint clearance in the process of motion, which will affect the positioning accuracy of the manipulator and cause large errors. Taking joint 6(the end of manipulator) as an example, the impact of the collision model on the motion of the robotic arm is considered for simulation analysis, which is shown as Figure 3.

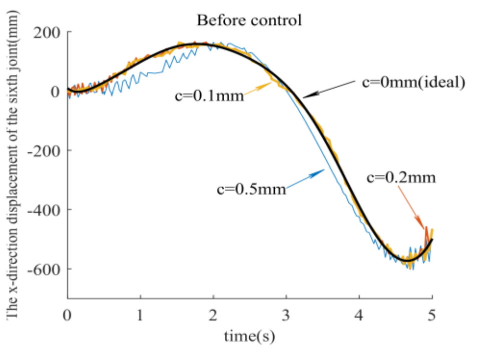

(a) The x-direction displacement of the sixth joint

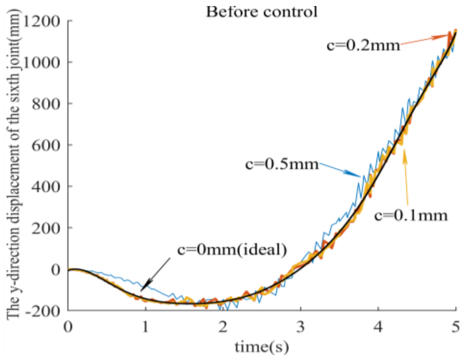

(b) The y-direction displacement of the sixth joint

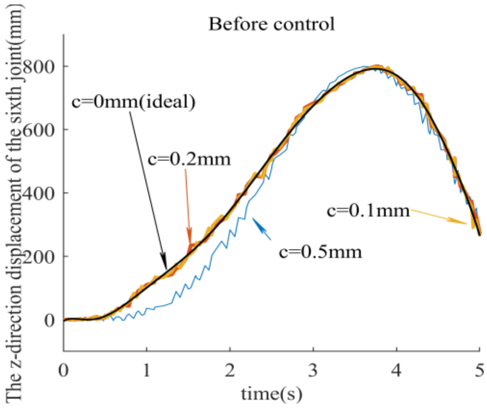

(c) The z-direction displacement of the sixth joint

Fig. 3. (a), (b), (c) The displacement of sixth joint before control.

By comparing different joint clearances, the displacement curves are drawn. It can be seen that the size of the clearance has a significant impact on the movement of the manipulator arm. The reason for this phenomenon is that the larger the gap is, the greater the velocity mutation, the greater the collision force, the more severe the collision degree and the more severe the vibration of the system are. Therefore, it is necessary to control the torque to reduce the impact force.

2.5 Modal analysis

According to the modal shape, the natural frequency and mode of vibration of the mechanical arm that both not affected by the external environment can be obtained, which can avoid the damage of the mechanical arm caused by resonance at a specific frequency. Therefore, the first six modes are selected for analysis according to the actual processing situation of the mechanical arm, which are shown as Table 2.

Table 2. First six frequencies and maximum deformation.

The order	Frequency/hz	The maximum deformation /mm
1	1.95	7.03
2	1.95	7.13
3	8.61	7.40
4	32.39	7.56
5	54.77	7.77
6	81.41	7.89

As can be seen from the Table 3 below, under different modes of vibration, the flexible joint of the manipulator deforms, the maximum deformation is not more than 7.9mm and the maximum stress is not more than 543MPa.At the same time, the first and second maximum stresses occur at the threaded connection between joints and the third, fourth-order modal modes show the third and fourth joints along the z axis have bending deformation, and torsional deformation of 5,6 order modal model is in the end of arm. So end deformation produced by the vibration of mechanical arm is to be reckoned with, and end of the mechanical arm as an important position of processing contact with processed object, vibration control is particularly important.

Table 3. The first six modes.

Deformation	First order mode diagram	Second order mode diagram	Third order mode diagram
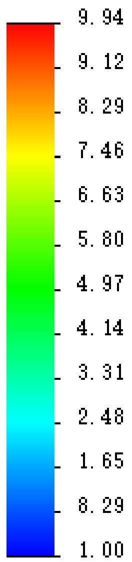	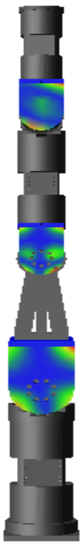	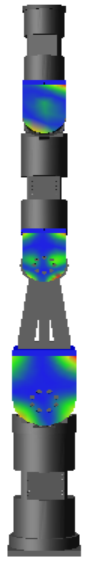	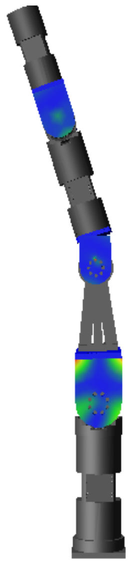
Fourth order mode diagram	**Fifth order mode diagram**	**Sixth order mode diagram**	**Maximum pressure**
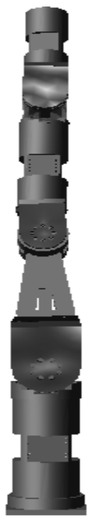	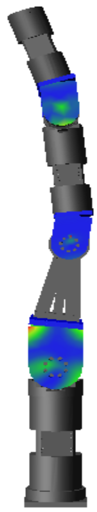		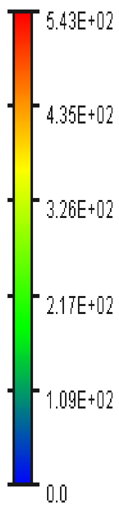

3. CONTROLLER DESIGN

Due to the joint clearance, when the joints of the robotic arm rotate, the collision force will generate impact and cause the joints to vibrate. An additional elastic device, namely a torsional spring damper, must be installed in the gap structure for direct compensation. After the joints are impacted, they can still maintain the original law of motion. In addition to adding a spring damper, it is also necessary to adjust the driving torque of each joint to reduce vibration. Therefore, the fish algorithm is selected to optimize PID parameters, combining PID control with the adaptive inversion of control, to adjust the driving torque of mechanical arm to achieve smooth movement.

3.1 Fish Swarm Algorithm

The fish swarm algorithm initializes the fish swarm to generate random numbers, and then uses the foraging behavior, clustering behavior, tailgating behavior and random behavior of the fish swarm itself to find the optimal parameters. The specific algorithm flow is shown in Figure 4.

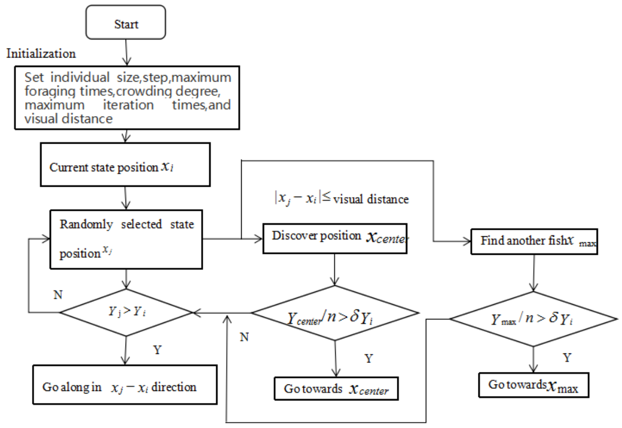

Fig. 4. Flowchart of fish swarm algorithm.

(1) The fish swarm is initialized first. Because PID parameters (k_p、k_i、k_d) are optimized, a random number group of 3 rows and n columns should be generated. (n is the total number of fish).

(2) In the foraging behavior, the state is randomly selected. If the state is increased, the state will continue; otherwise, the random state is re-selected and x_i set as the current state. x_j is another randomly selected state. The expression of foraging behavior can be defined as

$$x_i^{t+1} = x_i^t + \frac{x_j - x_i^t}{\left\| x_j - x_i^t \right\|} \cdot step \cdot rand(), \, y_i^{t+1} > y_i^t$$
$$x_i^{t+1} = x_i^t + step \cdot rand(), \, y_i^{t+1} \le y_i^t$$

(3)Judging the surrounding environment, if there are more objects in the partner center and the number of fish gathering is not large, swim in this direction, that is y_j ,on the contrary, perform foraging behavior and select x_j again, x_{center} is the center of the search area which meet the condition($d_{ij} \le visual$),and the expression can be defined as

$$x_i^{t+1} = x_i^t + \frac{x_{center} - x_i^t}{\left\| x_{center} - x_i^t \right\|} \cdot step \cdot rand(), y_i^{t+1} > y_i^t$$
$$\text{Step}(2), y_i^{t+1} \le y_i^t$$

(4) In order to avoid the local optimal solution, the foraging behavior direction is randomly generated.

(5) In order to find food quickly, the fish will follow other fish. The artificial fish will search within the range of $d_{ij} \le visual$ and find the fish $x_{\max}$ with the highest food concentration $y_{\max}$.When $\frac{y_{\max}}{n} > \delta y_i^t$, indicating that the fish receiving a relatively high concentration of food were not crowded around, the artificial fish swam towards $x_{\max}$,otherwise they performed foraging behavior

$$x_i^{t+1} = x_i^t + \frac{x_{\max} - x_i^t}{\left\| x_{\max} - x_i^t \right\|} \cdot step \cdot rand(), \frac{y_{\max}}{n} > \delta y_i^t$$
$$\text{Step}(2), \frac{y_{\max}}{n} \le \delta y_i^t$$

δ is the impact factor.

(6) The optimal solution of the parameters is substituted into the PID control block diagram as the parameters, and the torque is adjusted with the back control.

3.2 Adaptive Inverse Control

Compared with the traditional robust control (which can suppress interference and compensate unmodeled dynamics, but cannot learn autonomously), adaptive control has certain learning ability (Song et al., 2018). According to the input and output, parameters are constantly identified, and the real value of parameters is constantly approached through the adaptive law of parameters. Inversion method is to make the controller structured (Ahmed Elmogy, et al., 2020; Marques et al., 2017). It can also control the unfavorable nonlinear terms by using the favorable nonlinear terms of the system or increasing the nonlinear damping, so as to obtain better robust performance. When the inversion method and adaptive method is suitable for the state feedback linearization and the parameters of uncertain nonlinear systems. Through the parameter feedback in the form of nonlinear systems can be converted to solve the problem of the global stability and convergence by increasing the nonlinear term to improve the transition performance. In addition, by introducing virtual parameters, it can reduce the error and minimize the dimensions of the parameter estimation of convergence.

The above mentioned is the driving torque that directly drives the robot arm, but in practice it is driven by a motor. At the same time, the rotation angle and the rotation speed of the mechanical arm are also restricted (Nandor et al., 2021; Chuang, 2021). Therefore, it is necessary to ensure that the movement of the entire system is within the allowable error range. There are a large number of unknown nonlinear terms in the driving process of the motor, which are mainly caused by the external factors, such as external interference. However, changes in the parameters inside the motor can also cause interference, which leads to reduced control accuracy and even system control instability.

Firstly, two subsystems are designed to estimate the unknown nonlinearity of the system, and a new weighting law is designed according to the Lyapunov law, so that the estimated value of the entire subsystem can be close to the actual value. Then, the control system is designed based on the inverse control combined with the traditional Lyapunov function.

Therefore, in the case of parameter changes and external interference of the motor, the reconstruction of the system model is as follows:

$$\begin{cases} M\ddot{q} + C\dot{q} + G + D = T \\ K_T i = T \\ Li + Ri + K_e \dot{q} + P = U \end{cases} \tag{14}$$

Where C stands for the centrifugal force and Coriolis matrix, G represents the gravity matrix, D represents the unknown nonlinearity in the manipulator, which is less than the upper bound, T is the torque, i is the motor current, K_T is the conversion parameter between current and torque, L is the inductance, R is the resistance, K_e is the feedback coefficient of the motor, P is the unknown nonlinearity of the motor, which is less than its upper bound, and U is the input voltage.

In order to ensure that the position and velocity of the electrically driven manipulator system can quickly track the reference signal, and at the same time to ensure that the position and velocity errors of the system are always kept within the constraint range, a controller is designed to estimate the unknown nonlinear terms in the system to reduce its influence on the control. The joint angular velocity current is used as the state variable.

$$\begin{cases} x_1 = q \\ x_2 = \dot{q} \\ x_3 = i \end{cases} \tag{15}$$

Therefore, the system state equation is as follow:

$$\begin{cases} \dot{x}_1 = x_2 \\ \dot{x}_2 = M^{-1}(K_T x_3 - C x_2 - G - D) \\ \dot{x}_3 = L^{-1}(U - R x_3 - K_e x_2 - P) \\ y = x_1 \end{cases} \tag{16}$$

The position error and velocity error of the system are defined as

$$\begin{cases} e_1 = x_1 - x_d \\ e_2 = x_2 - \dot{x}_d \end{cases} \tag{17}$$

Use error and system state variables as inputs, under ideal conditions, $D = W_1^T \Phi(X) + \delta_1, P = W_2^T \Phi(X) + \delta_2$,W is the weight. $\Phi(X)=\exp\left[-\frac{\|X-\mu_i\|^2}{2\sigma_i^2}\right]$ is the Gaussian symmetric function, μ_i, σ_i is the center value of the Gaussian function and the center width value, respectively, and δ represents an error. Since the output value is constantly updated in the iterative process, the solution approaches the true value.

The errors of D and P are as follows,

$$\begin{aligned} e_D &= \tilde{W}_1^T \Phi(X)+\delta_1 \\ e_P &= \tilde{W}_2^T \Phi(X)+\delta_2 \end{aligned} \tag{18}$$

The inversion control block diagram is shown in Figure 5.

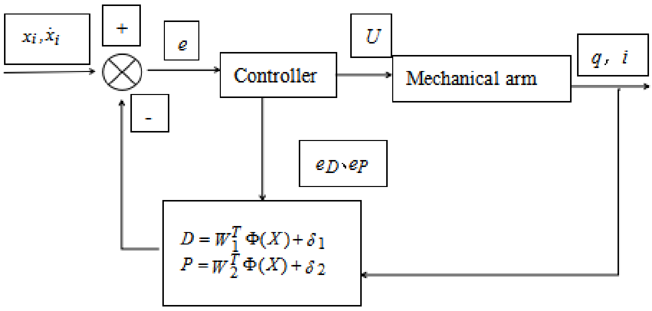

Fig. 5. Block diagram of system model.

Based on the idea of adaptive inverse control, the design process is to divide the nonlinear system into subsystems that do not exceed the order of the system, then design the Lyapunov function and the intermediate virtual control variables for the subsystem until they are completed, and finally assemble all the subsystems. The specific design steps are as follows:

Step 1

First define the position error signals

$$z_1 = x_1 - x_i \tag{19}$$

Then,

$$\dot{z}_1 = \dot{x}_1 - \dot{x}_i = x_2 - \dot{x}_i \tag{20}$$

The first Lyapunov function is

$$V_1 = \frac{1}{2}\ln\frac{b_1^2}{b_1^2 - z_1^T z_1} \tag{21}$$

Where b_1 is the constraint limit of the position, and the derivation of V_1 is as follows

$$\dot{V}_1 = \frac{z_1^T(x_2-\dot{x}_i)}{b_1^2 - z_1^T z_1} \tag{22}$$

Define virtual controls

$$a_1 = c_1 z_1 + \dot{x}_i \tag{23}$$

Define error signals

$$z_2 = x_2 - a_1 \tag{24}$$

Then

$$\dot{V}_1 = \frac{-c_1 z_1^T z_1}{b_1^2 - z_1^T z_1} + \frac{z_1^T z_2}{b_1^2 - z_1^T z_1} \tag{25}$$

where c_1 is a constant and greater than zero.

When z_2 is equal to zero, $\dot{V}_1 \le 0$;while z_2 is not always equal to zero, it is necessary to introduce a virtual control variable α_2 , which makes z_2 equal to zero.

Step 2

Differentiate with respect to z_2 ,

$$\dot{z}_2 = M^{-1}(K_T x_3 - C\dot{q} - G - D) - \dot{a}_2 \tag{26}$$

Take the second Lyapunov function

$$V_2 = V_1 + \frac{1}{2}\ln\frac{b_2^2}{b_2^2 - z_2^T z_2} + \frac{1}{2} z_2^T M z_2 \tag{27}$$

Where b_2 is the speed limit, which is a positive integer.

Differentiate with respect to V_2,

$$\begin{aligned} \dot{V}_2 = &-\frac{c_1 z_1^T z_1}{b_1^2 - z_1^T z_1} + \frac{z_1^T z_2}{b_1^2 - z_1^T z_1} + \frac{z_2^T \dot{z}_2}{b_2^2 - z_2^T z_2} \\ &+ z_2^T(K_T x_3 - C a_2 - G - D - M\dot{a}_2) \end{aligned} \tag{28}$$

Introduce another virtual control

$$\begin{aligned} a_2 = K_T^{-1}\Big(&-\frac{z_1}{b_1^2 - z_1^T z_1} - \frac{\dot{z}_2}{b_2^2 - z_2^T z_2} - c_{22} z_2 + G \\ &+ C a_2 + M\dot{a}_2 + e_D\Big) \end{aligned} \tag{29}$$

Set the error $z_3 = x_3 - a_3$ and substitute into $\dot{V}_2$,

$$\begin{aligned} \dot{V}_2 = &-\frac{c_1 z_1^T z_1}{b_1^2 - z_1^T z_1} - \frac{c_{21} z_2^T z_2}{b_2^2 - z_2^T z_2} \\ &- c_{22} z_2^T z_2 - z_2^T e_D + z_2^T K_T z_3 \end{aligned} \tag{30}$$

Step 3

Differentiate with respect to z_3 ,

$$\dot{z}_3 = L^{-1}(U - R x_3 - K_e x_2 - P) - \dot{a}_3 \tag{31}$$

Use the Lyapunov function for the third subsystem

$$V_3 = V_2 + \frac{1}{2} z_3^T L z_3 \tag{32}$$

Differentiate with respect to V_3,

$$\begin{aligned} \dot{V}_3 = &-\frac{c_1 z_1^T z_1}{b_1^2 - z_1^T z_1} - \frac{c_{21} z_2^T z_2}{b_2^2 - z_2^T z_2} - c_{22} z_2^T z_2 - z_2^T e_D \\ &+ z_2^T K_T z_3 + z_3^T(U - R x_3 - K_e x_2 - P - L\dot{a}_3) \end{aligned} \tag{33}$$

Design voltage control law

$$U = R x_3 + K_e x_2 + L\dot{a}_2 - K_T z_2 - c_3 z_3 + e_P \tag{34}$$

Substitute U into $\dot{V}_3$

$$\dot{V}_3 = -\frac{c_1 z_1^T}{b_1^2 - z_1^T z_1} - \frac{c_{21} z_2^T z_2}{b_2^2 - z_2^T z_2} - c_{22} z_2^T z_2 - c_3 z_3^T z_3 - z_2^T e_D - z_3^T e_P \tag{35}$$

Take the final Lyapunov function,

$$V = V_3 + \frac{1}{2\gamma_1}\tilde{W}_1^T \tilde{W}_1 + \frac{1}{2\gamma_2}\tilde{W}_2^T \tilde{W}_2 + \frac{1}{2\gamma_3}\delta_1^T \delta_1 + \frac{1}{2\gamma_4}\delta_2^T \delta_2 \tag{36}$$

Take the derivative of the above formula, the result is as follows

$$\begin{aligned} \dot{V} = &-\frac{c_1 z_1^T z_1}{b_1^2 - z_1^T z_1} - \frac{c_{21} z_2^T z_2}{b_2^2 - z_2^T z_2} - c_{22} z_2^T z_2 - c_3 z_3^T z_3 \\ &- z_2^T(\tilde{W}_1^T \Phi(X) + \delta_1) - z_3^T(\tilde{W}_2^T \Phi(X) + \delta_2) \\ &- \frac{1}{\gamma_1}\tilde{W}_1^T \dot{W}_1 - \frac{1}{\gamma_2}\tilde{W}_2^T \dot{W}_2 - \frac{1}{\gamma_3}\delta_1^T \dot{\delta}_1 - \frac{1}{\gamma_4}\delta_2^T \dot{\delta}_2 \end{aligned} \tag{37}$$

The weights are updated as follows

$$\begin{aligned} \dot{W}_1 &= -\gamma_1 z_2^T \Phi(X) - \omega_1 W_1 \\ \dot{W}_2 &= -\gamma_2 z_3^T \Phi(X) - \omega_2 W_2 \end{aligned} \tag{38}$$

The error is updated as follows

$$\begin{aligned} \dot{\delta}_1 &= -\gamma_3 z_2 \\ \dot{\delta}_2 &= -\gamma_4 z_3 \end{aligned} \tag{39}$$

Substitute $\dot{V}$,

$$\begin{aligned} \dot{V} = &-\frac{c_1 z_1^T z_1}{b_1^2 - z_1^T z_1} - \frac{c_{21} z_2^T z_2}{b_2^2 - z_2^T z_2} - c_{22} z_2^T z_2 - c_3 z_3^T z_3 \\ &- \frac{\omega_1}{\gamma_1}\tilde{W}_1^T \tilde{W}_1 - \frac{\omega_2}{\gamma_2}\tilde{W}_2^T \tilde{W}_2 + \frac{\omega_1}{\gamma_1}\tilde{W}_1^T W_1 + \frac{\omega_2}{\gamma_2}\tilde{W}_2^T W_2 \end{aligned} \tag{40}$$

The purpose of the design is to ensure that the controller designed with the Lyapunov function can satisfy the position and speed of the entire system, and at the same time, the error is always kept within a limited range. Then the design of the subsystems is to estimate the unknown nonlinear terms in the system and to minimize the impact on the control effect. By following the above steps, the design of the virtual control law can ensure the stability, then modify it step by step, and then a real controller is designed to achieve overall control and meet the purpose of controlling the amplitude of the vibration wave within a certain range until smooth.

4. SIMULATION AND EXPERIMENTS

In order to verify the effectiveness of the adaptive inverse controller, a control block diagram was designed using MATLAB/ Simulink module, and the dynamics simulation of the 6-DOF flexible joint manipulator was carried out using the above-designed controller.

In order to complete the optimization of PID parameters, it is necessary to establish the vibration control of the flexible joint manipulator composed of an objective function, a simulation model and a PID controller. The fish swarm algorithm is combined with the following Figure 6 to set the objective function, that is, the relationship between the system input and output in the PID controller.

$$u(t) = K_p e(t) + K_i \sum_{n=0}^{t} e(n) + K_d(e(t) - e(t-1))$$

the sensing range of the artificial fish swarm is set to 1, the movable step size is set to 0.1, the number of the artificial fish swarm is 50, and the status of the fish state $[K_p、K_i、K_d]$ is [(-20,20),(-30,30),(30,30)], respectively. The simulation was conducted based on the above algorithms and the optimal solutions of the parameters were obtained, which are 10,23 and 25 respectively. The results of fish swarm algorithm are be shown in Figure 7.

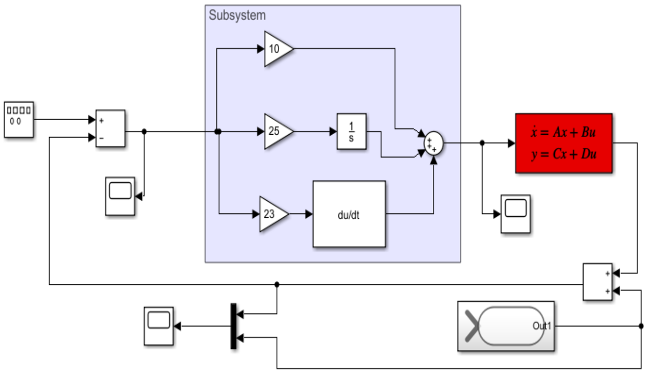

Fig. 6. Block diagram of fish swarm algorithm and PID control.

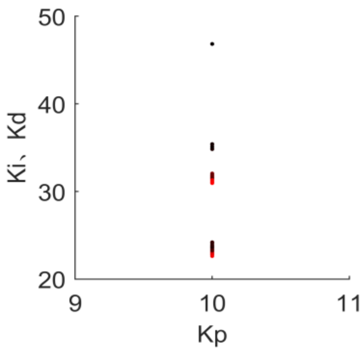

Fig. 7. Fish swarm algorithm result graph (The distance between the red dots represents the optimal solution size).

After the optimal solution is obtained, the PID control parameters are substituted. Torque is applied to each joint in advance, and PID is combined with adaptive inverse control to obtain the control curve of torque. The Figure 8 is the overall control block diagram.

Under the real experimental conditions, as it can be seen from the Figure 9, when the flexible joint is subjected to the impact force, the impact vibration is generated. In the absence of torque control, the pre-applied torque generates different amplitudes when the collision occurs, and the maximum amplitude of the fluctuation can exceed 30N·mm. After the torque control, the peak torque of the first joint is significantly alleviated, while the amplitude of the second joint torque is significantly decreased compared with that of the first joint torque. The maximum amplitude of the torque is controlled within 1.2N·mm. Meanwhile, the vibration peak decreases with the simulation time goes on. The torque amplitudes of the third, fourth, fifth joints decreased significantly and were controlled within 0.1N·mm, 0.1N·mm and 0.08N·mm respectively. The torque of the end joints of the manipulator were basically unchanged, proving the effectiveness of the method. The overall joint torque curves were basically stable after 3s (when the first vibration occurred). After torque control, the most direct judgment of the advantages and disadvantages of the control method is to analyze the stability of the end joint and select the end joint as an example, because as the closest joint to the processed surface, its vibration will be triggered by external interference and the change of its own parameters, which will directly affect the quality of the processed surface. Therefore, the control of the terminal joint by the controller represents the control of all other joints and the overall control precision.

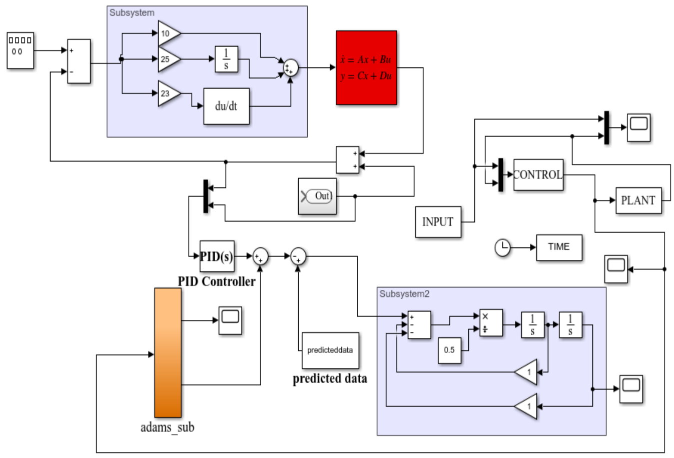

Fig. 8. The control block diagram.

(a) Experimental equipment diagram

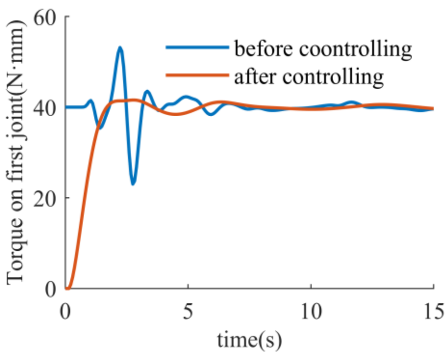

(b) The first joint torque control diagram

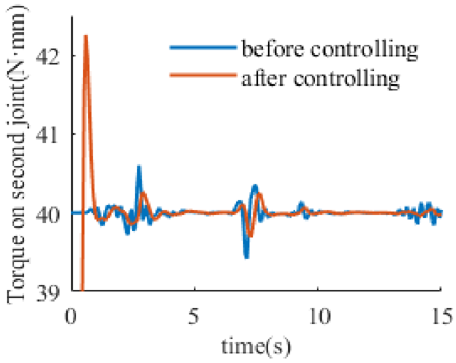

(c) The second joint torque control diagram

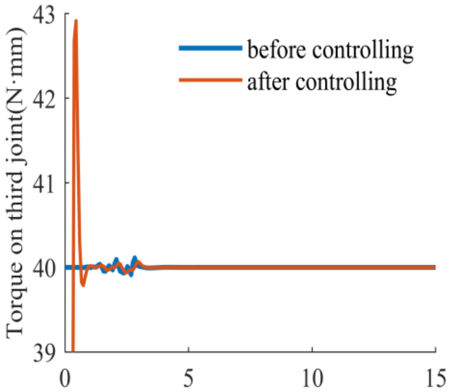

(d) The third torque control diagram

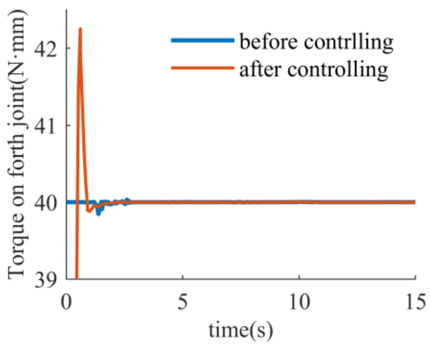

(e) The fourth joint torque control diagram

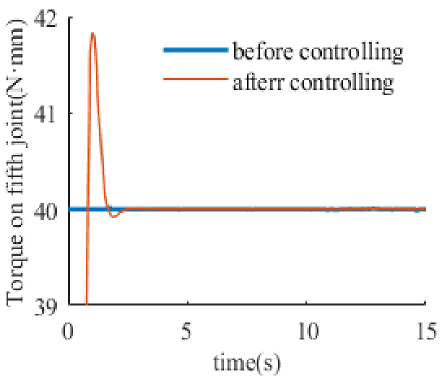

(f) The fifth joint torque control diagram

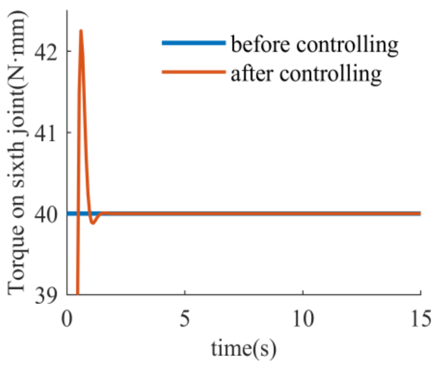

(g) The sixth joint torque control diagram

Fig. 9(a)~(g). The Experimental equipment diagram and torque control diagram.

The deviation of the ideal articulated pair with different joint gap size after control (Fig. 10) is compared with the displacement before (Fig. 3) control. It can be seen that no matter how big or small clearance, compared with the displacement control before and after the control of the displacement and the ideal situation is more close to latter, which further confirmed the feasibility and effectiveness of this method. At the same time the deformations of mechanical arm after control was also significantly reduced, which are shown in Table 4.

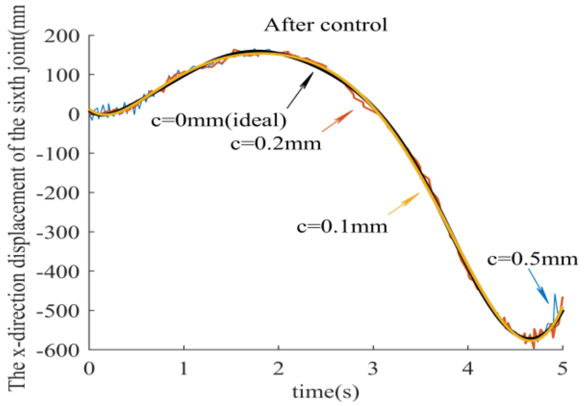

(a) The x-direction displacement of the sixth joint

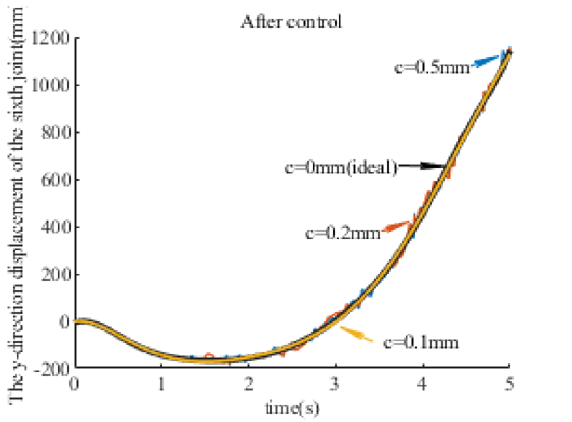

(b) The y-direction displacement of the sixth joint

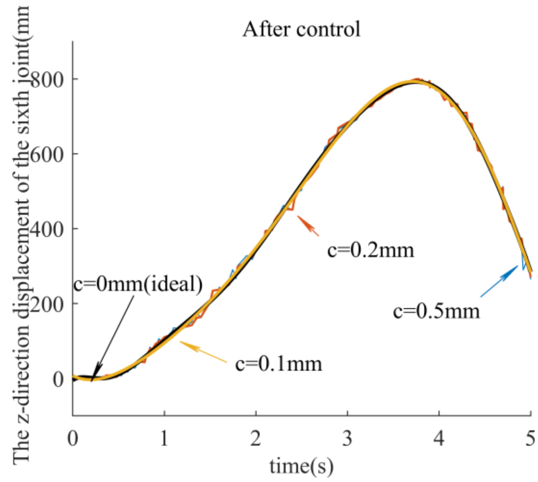

(c) The z-direction displacement of the sixth joint

Fig. 10(a), (b), (c). The displacement of the sixth joint after control.

Table 4. Maximum deformation of each stage

The order	Maximum/mm
1	0.02
2	0.03
3	0.2
4	0.97
5	1.2
6	1.5

5.CONCLUSIONS

(1) The joint clearance caused by design or assembly causes the impact of the flexible joint in the rotation process. In order to maintain the original trajectory of the manipulator and take the moment as the starting point, a control method is proposed to optimize the PID parameters by using the fish swarm algorithm and combine it with the improved adaptive inverse control.

(2) Considering the mechanism containing the driving motor, the stepwise control strategy is designed using the inversion method, considering the modeling error and the motor voltage interference term, and the weight adaptive law is designed based on the Lyapunov function for online adjustment and compensation.

(3) The simulation results show that the proposed control method can improve the vibration impact caused by the collision during the movement of the flexible joint. The amplitude of torque fluctuation can be reduced to less than 0.1N·mm from the minimum, and the response time is short. For the fluctuation segment with large vibration amplitude, the amplitude can be reduced within 1s, and the response speed is fast At the same time, it is proved that the gap size after control has little influence on the displacement of the end joint of the manipulator, which ensures its accuracy.

(4) Some influencing factors have been neglected, and should be further studied in the future, such as the coupling effect between different rotation pairs, especially the rotation direction and the different rotation speed, and the influence of forces during machining on joints. And these factors could provide new insights, when considering the actual machining process.

REFERENCES

Adelhedi, F., Jribi, A., Bouteraa, Y. and Derbel, N. (2015). Adaptive sliding mode control design of a SCARA robot manipulator system under parametric variations. *Journal of Engineering Science and Technology Review*, Volume 5, No. 15, 17-123.

Ahmed Elmogy, Yassine Bouteraa, and Wael Elawady (2020). An Adaptive Fuzzy Self-Tuning Inverse Kinematics Approach for Robot Manipulators. *Journal of control engineering and applied informatics*., 22(4): 43-51

Arz´en, K.E. (1999). A simple event-based PID controller. *In Preprints of the 14th World Congress of IFAC*.

Chien M.C., Huang A.C. (2007). Adaptive control for flexible-joint electrically driven robot with time-varying uncertainties. *IEEE Transactions on Industrial Electronics*, 54(2), 1032-1038.

Chuang W-L, Yeh M-H, Yeh Y-L. (2021) Develop Real-Time Robot Control Architecture Using Robot Operating System and Ether CAT. *Actuators*. 10(7):141.

Chung J, Hulbert G M. (1993). A time integration algorithm for structural dynamics with improved numerical dissipation: The generalized-method. *Journal of Applied Mechanics-Transactions of the ASME*, 60(2):371-375.

Fateh M.M., Kashani M.S. (2013). Decentralized direct adaptive fuzzy control for flexible-joint robots, *Journal of control engineering and applied informatics*, 15(4), 97- 105.

Guo, Y. and Woo, P.Y. (2003). An adaptive fuzzy sliding mode controller for robotic manipulators. Systems, Man and Cybernetics, Part A: Systems and Humans, *IEEE Transactions on*, 33(2), 149－159.

Huang A.C., Chen Y.C. (2004). Adaptive sliding control for single-link flexible-joint robot with mismatched uncertainties,” *IEEE Transactions on Control System Technology*, 12(5), 770－775.

Marques F, Souto A P, Flores P. (2017). On the constraints violation in forward dynamics of multibody systems. *Multibody System Dynamics*, 39(4):385-419.

Mircea Niţulescu (2007) Solutions for modeling and control in mobile robotics, *Journal of control engineering and applied informatics*,9(3,4):43-50.

Mustapha, L., Benyamine, A., Abdelhafid, O., Dequidt, A., and Vermeiren, L. (2014). Sliding mode control of biglide planar parallel manipulator. In Automation and Robotics. Proceedings, *2014 ICINCO International Conference on*, 303–310. ICINCO.

Nandor MJ, Heebner M, Quinn R, Triolo RJ, Makowski NS. (2021) Transmission Comparison for Cooperative Robotic Applications. *Actuators*.10(9):203.

Omer S., Faisal A., Muhammad U. K., Muhammad A. I., Salman K. (2018). Adaptive Collaborative Position Control of a Tendon-Driven Robotic Finger. *Journal of control engineering and applied informatics*,20(2):87-99.

Ortega R, Orden J C G, Cruchaga M, et al.(2017). Energy-consistent simulation of frictional contact in rigid multibody systems using implicit surfaces and penalty method. *Multibody System Dynamics*, 41(3):275-295.

Prakash, J. and Srinivasan, K. (2009). Design of nonlinear PID controller and nonlinear model predictive controller for a continuous stirred tank reactor. *ISA Transaction*, 48, 273-282.

R. Kalaivani, P. Lakshmi, (2014). Biogeography-Based Optimization of PID Tuning Parameters for the Vibration Control of Active Suspension System, *Journal of control engineering and applied informatics*,16(1),31-39.

Rajinikanth, V. and Latha, K. (2012). Controller Parameter Optimization for Nonlinear Systems Using Enhanced Bacteria Foraging Algorithm. *Hindawi Publishing Corporation Applied Computational Intelligence and Soft Computing*, 2012, 1-12.

Sefriti S., Boumhidi J., Naoual R., Boumhidi I. (2012). Adaptive neural network sliding mode control for electrically-driven robot manipulators. *Journal of control engineering and applied informatics*, 14(4), 27-32.

Shengli, Song., Yuxuan, Cao, Haitao Wang, et al (2018). Adaptive Output Feedback Force Tracking Control for Lower Extremity Power Assisted Exoskeleton, *Journal of control engineering and applied informatics,* 20(3):60-68.

Sylvain D,, Bruno B,, Nicolas M,, J. Fermi G.C.,(2018). Event-Based PID Control: Application to a Mini Quadrotor Helicopter*, Journal of control engineering and applied informatics*,20(1):36-47.

Talebi H.A., Patel R.V., Wong M. (2002). A neural-network based observer for flexible-joint manipulators. *IFAC, 15th Triennial World Congress*, Spain.

Vermeiren, L., Dequidt, A., Afroun, M., and Guerra, T.M. (2012). Motion control of planar parallel robot using the fuzzy descriptor system approach. *ISA transactions*, 51(5), 596–608.

Yang, Z., Wu, J., and Mei, J. (2007). Motor-mechanism dynamic model based neural network optimized computed torque control of a high speed parallel manipulator. *Mechatronics*, 17(7), 381–390.

Zhou H., Chen R., Zhou S. and Liu Z. (2019). Design and analysis of a drive system for a series manipulator based on orthogonal-fuzzy PID control. *Electronics Journal*. 8(9), 1051.

Zirkohi M.M, Fateh M.M., Shoorehdeli M.A. (2013). Type-2 fuzzy control for a flexible-joint robot using voltage control strategy. *International Journal of Automation and Computing*, 10(3), 242-255.